This article has been accepted for publication in a future issue of this journal, but has not been fully edited. Content may change prior to final publication. Citation information: DOI 10.1109/TIE.2018.2886765, IEEE Transactions on Industrial Electronics

Framework of Gradient Descent Least Squares Regression Based NN Structure for Power Quality Improvement in PV Integrated Low-Voltage Weak Grid System

Nishant Kumar, *Member IEEE*, Bhim Singh, *Fellow IEEE*, and Bijaya Ketan Panigrahi, *Senior Member IEEE*

***Abstract*—This work proposes a novel gradient descent least squares regression (GDLSR) based neural network (NN) structure for control of grid-integrated solar PV (Photovoltaic) system with improved power quality. Here, a single layer neuron structure is used for the extraction of fundamental component (FC) from the load current. During FC extraction, GDLSR based NN structure attenuates harmonic components, noise, DC offsets, bias, notches and distortions from the nonlinear current, which improves the power quality under normal as well as under abnormal grid conditions. This single layer GDLSR-based NN structure has a very simple architecture, which decreases the computational burden and algorithm complexity. Therefore, it is easy in implementation. In this work, the GDLSR based control technique is tested on a single-phase single-stage grid-integrated PV topology with the nonlinear loads. The prime objective of the GDLSR based NN structure is to provide reactive power compensation, power factor correction, harmonics filtering and mitigation of other power quality issues. Moreover, when solar irradiation is zero, then the DC link capacitor and VSC, act as a distribution static compensator (DSTATCOM), which enhances the utilization factor of the system. The proposed system is modelled, and its performances are verified experimentally on a developed prototype in different grid disturbances as well as solar insolation variation conditions, which performances have satisfied the motive of proposed technique as well as the IEEE-519 standard.**

***Index Terms*—Solar Energy, Grid Integration, DSTATCOM, GDLSR based Control, Single-phase Grid, Single-stage Topology, Power Quality.**

I. INTRODUCTION

THE use of solar PV (Photovoltaic) generation for rural electrification, is growing very rapidly. The popularity of solar PV generation in the rural area, is due to its static nature, easy installation, low maintenance, and zero fuel cost. Therefore, government, as well as nongovernmental organizations, are installing or supporting the installation of rooftop PV system in rural areas for continuous electricity. These schemes are also popular in the urban areas, because they help to the user in monthly electricity charge reduction and help to the utility during peak loading [1]. However, the success and robustness of the solar PV power generation (SPVPG), depend on control technique, which integrates the SPVPG system to the grid as well as maintains the power quality, through behaving as a distribution static compensator (DSTATCOM) [2]. The DSTATCOM action of it, provides reactive power compensation, power factor correction, harmonics filtering and mitigation of other power quality issues. Moreover, when solar irradiation is zero, then the DC link capacitor and VSC (Voltage Source Converter), act as a DSTATCOM [2], which enhances the utilization factor of it. Therefore, all responsibilities are on the control technique.

In recent time, neural network (NN) based control techniques have become popular [3]. Because recent advancement in NN has reduced the computational burden and algorithm complexity. Therefore, wide range NN based control techniques are used in the online system [4][5]. In order to make control fast and to increase the decision taking ability, NN based control techniques are highly popular in grid integration system [6]. Today, due to generic nature and parallelized computation, frequently NN has been applied in almost every control technique. Xie *et al.* [7] have given NN based adaptive dynamic programming control in the scheduling of vehicle-to-grid system. Mishra [8] has proposed an updating of NN- based technique for an unified power flow controller. Agarwal *et al.* [9] have proposed the least mean square based NN structure for control purpose in the distribution network. Venayagamoorthy *et al.* [10] have proposed dynamic adaptive programming for the smart micro-grid application. Similarly, some literature is available, where NN is integrated with conventional control technique.

In-depth literature review on ‘control techniques for the grid integrated solar PV system’ depicts that several novel fundamental extraction, harmonics elimination and synchronization techniques have been proposed for efficient control of grid integrated solar PV system. The *dq0*-transformation based SRF (Synchronous Rotating Frame) [11] control technique is a most popular technique. Because, in normal condition, it performs very good UPF (Unity Power Factor) operation or reactive power support to the grid. However, due to load unbalances, the second harmonic component is dominant in *dq0*-components. Therefore, for mitigation of second harmonic component, a low-pass filter is used, which slows down the performances of SRF based control technique. Moreover, recently, researchers have proposed several adaptive control algorithms, such as fuzzy adaptive control, learning based control, power delta control etc. However, at abnormal grid conditions, the performances of these control techniques, are not reported, which is the essential phenomenon of the distribution grid. The other control techniques like, discrete-Fourier transform (DFT) [12], PM (Prony’s method) [13], frequency locked loop (FLL), second-order generalized integrator (SOGI) [14] and Kalman filter (KF) [15] have been proposed to handle the abnormal grid conditions. However, none of these techniques, is suitable for all types of grid adverse conditions, such as FLL and SOGI based control techniques are unable to handle lower order harmonics and DC offset. The fixed length window with stationary waveform is required for searching in DFT based control technique, which is not suitable for online searching. The performance of PM is appreciable in different grid adverse conditions. However, in the PM technique, the higher

This article has been accepted for publication in a future issue of this journal, but has not been fully edited. Content may change prior to final publication. Citation information: DOI 10.1109/TIE.2018.2886765, IEEE Transactions on Industrial Electronics

order polynomial equation and its solution process, create a huge computational burden on the processor, which is not suitable for the low-cost microcontroller. Similarly, KF based control technique is good for estimation using correction and prediction process. Moreover, the modified version of KF, like extended KF and linear KF based control techniques, is also good for the PV integrated grid system. However, during state variable estimation, linearization, prediction and correction, the derivative properties are used, which is the source of burden and algorithm complexity on the processor. Therefore, a heavy computational burden arises on the processor, which is not suitable for a low-cost microcontroller. Model predictive control technique is also popular for good steady-state response, but during dynamic condition, its responses are poor, due to its predictive nature, which is based on the previous dataset. Similarly, resonant controllers, for tracking the sinusoidal inverter current in the grid-connected system [16], show a good steady state response with low harmonics content in injected grid current. However, during the transient condition, performance rapidly deteriorates, due to the changes in the grid frequency [17].

Recently, several adaptive control algorithms have been developed, like discrete Fourier transform, SOGI [14], FLL, KF [15], least mean square [18], least mean fourth (LMF) [19], Leaky LMF [20] etc. However, the major issues with these techniques are that the performances of these algorithms are not examined under abnormal grid conditions, those are most frequent, unusual and critical phenomenon in distributed power generation system.

Therefore, in this paper, a novel gradient descent least squares regression (GDLSR) based control algorithm is developed for robust and efficient control of grid-tied solar PV array system. GDLSR technique belongs to the affine projection family, where Laplacian kernel function [21] is integrated into weight updating process for quick pattern recognition of fundamental component. Due to the hybridization of gradient descent vector with least squares regression, this technique is free from the derivative term, so the computational burden is low, as well as the performance of GDLSR control is instantaneous and suitable for the high-frequency system.

The performance of GDLSR is tested on the single phase single stage grid-connected solar PV system, where loads are connected at the PCC (Point of Common Coupling) [22]. During testing, nonlinear loads are considered, and tested over every possible conditions, such as during irradiation changing condition, nonlinear load variation. Moreover, when PV power generation is more than the load demand, then extra power is supplied to the grid, and considered grid conditions are, grid over-voltage, grid under-voltage, harmonics in grid voltage. Moreover, it is tested on low solar irradiation, when PV power generation is less than the required load demand, then to fulfil the load demand, extra power is drowned from the grid. However, when solar irradiation is zero, then the system operates like DSTATCOM [23]. These all functions are performed on the developed prototype, and demonstrated through test results as well as proven by analysis on the IEEE-519 standard.

A. *Contribution*

The salient features of this work, are as follows:

- A novel gradient descent least squares regression based control algorithm is developed for robust and efficient performance of grid-integrated solar PV array system.
- The developed gradient descent least squares regression based control algorithm belongs to the affine projection family, where the Laplacian kernel function is integrated into the weight updating process for quick pattern recognition.
- The developed technique is validated experimentally in different adverse conditions, such as, over-voltage, under-voltage, distorted grid voltage, variable load condition, different types of solar irradiation variation condition etc.
- For an increase the utilization of the system, the control technique is developed in such a way that in daytime the system behaves like solar power fed grid integrated system, and in nighttime, this system behaves like DSTATCOM.

II. System Configuration

A single-stage topology of single-phase grid-tied solar PV system is given in Fig.1, where solar PV power is supplied to the grid, through a single-phase VSC in such a way that the operating point of PV array is at MPP (Maximum Power Point) and, the converter power is synchronized to the grid. Here for control, an incremental conductance (InC) MPPT algorithm [24], and GDLSR based control algorithm, are used for control of DC-AC VSC. In this configuration, at the PCC, ripple filter (C_{fl}, R_{fl}), the grid through interfacing inductor (L_{In}, R_{In}), and the output terminals of VSC are connected. Here, the ripple filter is used for absorbing switching ripples, which are produced by VSC. The main objective of the control scheme is during PV power generation, the available power is fed to the grid at UPF [25].

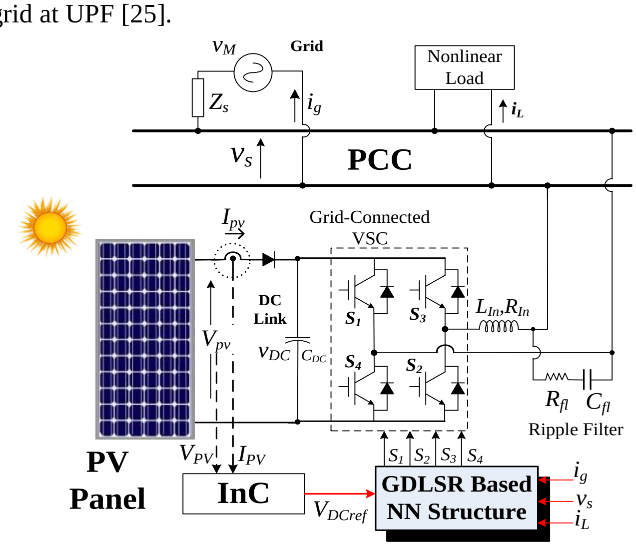

Fig.1 Grid-tied solar PV array.

III. Control Approach

In the proposed control scheme, a novel GDLSR based control strategy is used, where GDLSR algorithm is used for extraction of the fundamental component from load current. The GDLSSR based control strategy is shown in Fig.2.

First, InC MPPT technique is used, which produces a reference DC link voltage (V_{DCref}) for operating it on maximum power.

After this, by using a bandpass filter, the fundamental component of PCC voltage (v_{sp}) [22] is extracted from the grid voltage (v_s). This v_{sp} is in-phase quantity of v_s. The quadrature component (v_{sq}) of v_s is produced by shifting of $+\pi/2$ w.r.t. v_{sp}. The transfer function of bandpass filter is derived as,

$$T_f = \frac{k(z-1)}{z^2 + (k-2)\times z + \left(1-k+\frac{k^2}{2}\right)} \quad (1)$$

Where, $k=\sqrt{2}\times\omega\times T_s$, T_s and ω are sampling period and natural frequency ($2\pi f$), respectively.

The amplitude of v_s, unit-template in-phase (u_{ps}) [26] and a quadrature component (u_{qs}) are calculated as,

$$V_x = \sqrt{v_{sp}^{\ 2} + v_{sq}^{\ 2}} \quad (2)$$

$$u_{ps} = \frac{v_{sp}}{\sqrt{v_{sp}^{\ 2} + v_{sq}^{\ 2}}} \quad (3)$$

$$u_{qs} = \frac{v_{sq}}{\sqrt{v_{sp}^{\ 2} + v_{sq}^{\ 2}}} \quad (4)$$

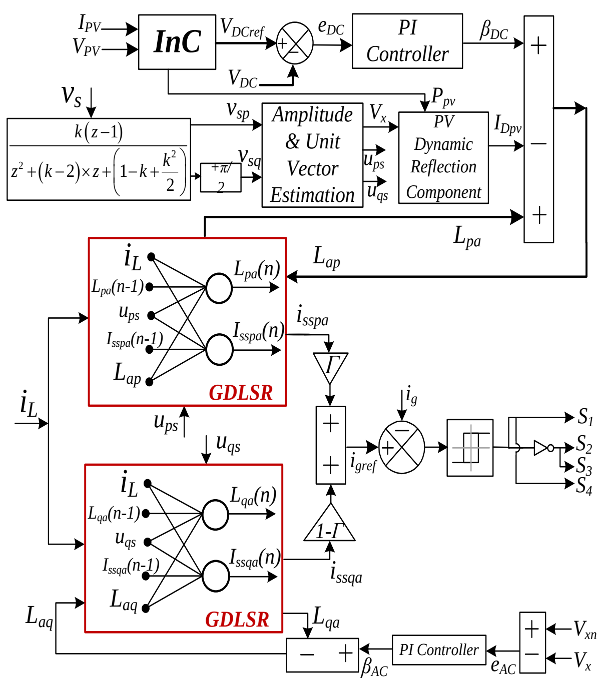

Fig.2 Control scheme for single-stage single-phase grid-connected PV system.

For improving the dynamic performances, by using the solar PV dynamic reflection component (I_{Dpv}), the impact of instantaneous reflection in solar power (P_{PV}) on i_g is considered, which is derived as,

$$I_{Dpv} = \frac{2\times P_{pv}}{\sqrt{v_{sp}^{\ 2} + v_{sq}^{\ 2}}} \quad (5)$$

For maintaining the DC link voltage, V_{DCref} is compared with the sensed DC link voltage (V_{DC}), which generates DC link voltage error ($e_{DC}= V_{DCref} - V_{DC}$). This e_{DC} is fed to the PI (Proportional Integral) controller, which gives the value of the DC loss component (β_{DC}), as,

$$\beta_{DC}(n+1) = G_P \times e_{DC}(n) + G_I \sum_{n=0}^{t} e_{DC}(n) \quad (6)$$

Where, G_P and G_I are proportional and integral gains of the PI controller, which regulates the *DC* link voltage.

For maintaining the v_{PCC} (PCC voltage) [22], reference PCC voltage (V_{xn}) is compared with the sensed PCC voltage (V_x), which generates AC link voltage error ($e_{AC}= V_{xn} - V_x$). This e_{AC} is fed to the PI controller, which gives the value of the AC loss component (β_{AC}), as,

$$\beta_{AC}(n+1) = G_{Pa} \times e_{AC}(n) + G_{Ia} \sum_{n=0}^{t} e_{AC}(n) \quad (7)$$

Where, G_{Pa} and G_{Ia} are proportional and integral gains of the PI controller, that regulates v_{PCC}.

For generating active (i_{sspa}) and reactive (i_{ssqa}) components of reference grid current, as well as for generating estimated active (L_{pa}) and reactive weight component (L_{qa}), two separate GDLSR control blocks are used, which are the function of load current (i_L), u_{ps}, u_{qs}, resultant active weight component (L_{ap}), and resultant reactive weight component (L_{aq}).

$$\left.\begin{array}{l} [i_{sspa},\ L_{pa}] \Rightarrow f_{GDLSR}(i_L, u_{ps}, L_{ap}) \\ [i_{ssqa},\ L_{qa}] \Rightarrow f_{GDLSR}(i_L, u_{qs}, L_{aq}) \end{array}\right\} \quad (8)$$

Where L_{ap} and L_{aq} are calculated as,

$$L_{ap} = \beta_{DC} + L_{pa} - I_{Dpv} \quad (9)$$

$$L_{aq} = \beta_{AC} - L_{qa} \quad (10)$$

The reference i_g (i_{gref}) is produced as,

$$i_{gref} = \Gamma \times i_{sspa} + (1-\Gamma) \times i_{ssqa} \quad (11)$$

Where, for UPF operation, Γ=1, and for reactive power support operation Γ=0, means at a time only one operation is performed.

The switching pulses (S_1, S_2, S_3, and S_4) of the voltage source converter are generated by using a hysteresis controller, where the input signals are i_{gref} and i_g.

A. Incremental Conductance Algorithm

The efficiency of the solar PV array is improved by using a MPPT algorithm, which forces to operate it at the maximum power point. The most popular MPPT technique, InC [24] is used here, because it is easy in implementation. The logic of InC is as follows,

$$\left.\begin{array}{l} if\ \partial v_{PV}=0, \begin{cases} if\ \ \partial i_{PV}=0, & then\ V_{DCrefnew}=V_{DCrefold} \\ else\ if\ \partial i_{PV}>0, & then\ V_{DCrefnew}=V_{DCrefold}-\Delta\xi \\ else\ V_{DCrefnew}=V_{DCrefold}+\Delta\xi \end{cases} \\ else, \begin{cases} if\ \partial i_{PV}/\partial v_{PV}=-i_{PV}/v_{PV}, & then\ V_{DCrefnew}=V_{DCrefold} \\ else\ if\ \partial i_{PV}/\partial v_{PV}>-i_{PV}/v_{PV}, & then\ V_{DCrefnew}=V_{DCrefold}+\Delta\xi \\ else\ V_{DCrefnew}=V_{DCrefold}-\Delta\xi \end{cases} \end{array}\right\} \quad (12)$$

Where, $\Delta P_{pv}=P_{PVnew}-P_{PVold}$, $\Delta v_{pv}=v_{PVnew}-v_{PVold}$, and $\Delta\xi$ is step change of reference DC voltage.

❖ The pseudo code for InC is given as follows,

begin (InC)

$\Delta i_{pv} = i_{pvnew} - i_{pvold}$;

$\Delta v_{pv} = v_{PVnew} - v_{PVold}$;

If $(\Delta v_{pv} = 0)$

This article has been accepted for publication in a future issue of this journal, but has not been fully edited. Content may change prior to final publication. Citation information: DOI 10.1109/TIE.2018.2886765, IEEE Transactions on Industrial Electronics

If $(\Delta i_{pv} \neq 0)$
If $(\Delta i_{pv} > 0)$
$V_{DCrefnew} = V_{DCrefold} + \Delta\xi$
else $V_{DCrefnew} = V_{DCrefold} - \Delta\xi$; *end*
end
else
If $(\Delta i_{pv}/\Delta v_{pv} \neq - i_{pv}/ v_{pv})$
If $(\Delta i_{pv}/\Delta v_{pv} > - i_{pv}/ v_{pv})$
$V_{DCrefnew} = V_{DCrefold} - \Delta\xi$
else $V_{DCrefnew} = V_{DCrefold} + \Delta\xi$; *end*
end
end.

B. Gradient Descent Least Squares Regression (GDLSR) based NN Structure

The GDLSR technique is a hybrid of gradient descent vector with least squares regression, which belongs to the affine projection family. Moreover, here the Laplacian kernel function [21] is used for quick pattern recognition.

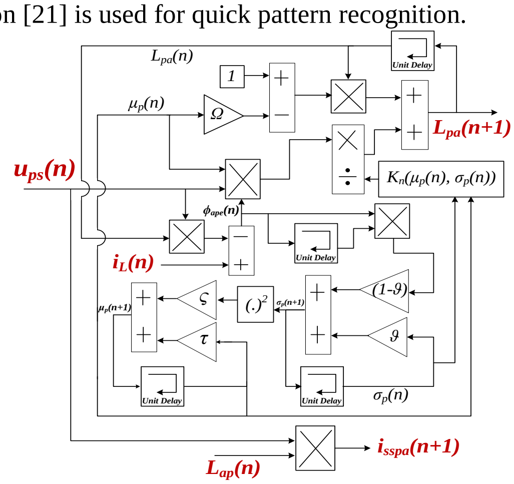

Fig.3 Block model of GDLSR for active weight component.

The GDLSR smoothly adjusts the conventional cost functions, which minimizes the tracking errors, improves quick pattern recognition, and filter performance. Here, prediction error (ϕ_{ape}) of the active weight component is derived as,

$$\phi_{ape}(\mathrm{n}) = i_L(\mathrm{n}) - \mathrm{u}_{ps}(n) \times L_{pa}(n) \tag{13}$$

Through proper adjustment and updating of active weight ($L_{pa}(n)$), the ϕ_{ape} is minimized, which is defined as,

$$L_{pa}(n+1) = \left(1 - \Omega \times \mu_p(n)\right) \times L_{pa}(n) + \frac{\mu_p(n) \times \mathrm{u}_{ps}(n) \times \phi_{ape}(n)}{K_n\left(\mu_p(n), \sigma_p(n)\right)} \tag{14}$$

Where, Ω is leaky learning rate of $L_{pa}(n)$, and Laplacian kernel function is K_n. σ_p(n) and $\mu_p(n)$ are autocorrelation factor and designed parameter, respectively, which give an additional degree of freedom.

Where, μ_p and K_n are described as,

$$K_n\left(\mu_p(n), \sigma_p(n)\right) = e^{-\Omega \times \left\| \mu_p(n) - \sigma_p(n) \right\|} \tag{15}$$

$$\mu_p(n+1) = \tau \times \mu_p(n) + \varsigma \times \left(\sigma_p(\mathrm{n}+1)\right)^2 \tag{16}$$

Where, τ and ς are accelerating parameters. The $\sigma_p(n)$ is described as,

$$\sigma_p(n+1) = \vartheta \times \sigma_p(n) + (1-\vartheta) \times \phi_{ape}(n) \times \phi_{ape}(n-1) \tag{17}$$

i_{sspa} is generated as,

$$i_{sspa} = L_{ap} \times u_{ps} \tag{18}$$

For easy and smooth implementation as well as better understanding, the block model of GDLSR, for $L_{pa}(n)$ and i_{sspa} generation is illustrated in Fig.3.

Similarly, the prediction error (ϕ_{aqe}) of the reactive weight component is derived as,

$$\phi_{aqe}(\mathrm{n}) = i_L(\mathrm{n}) - \mathrm{u}_{qs}(n) \times L_{qa}(n) \tag{19}$$

Through proper adjustment and updating of reactive weight ($L_{qa}(n)$), the ϕ_{aqe} is minimized, which is defined as,

$$L_{qa}(n+1) = \left(1 - \Omega \times \mu_q(n)\right) \times L_{qa}(n) + \frac{\mu_q(n) \times \mathrm{u}_{qs}(n) \times \phi_{aqe}(n)}{K_n\left(\mu_q(n), \sigma_q(n)\right)} \tag{20}$$

Where, Ω is leaky learning rate of $L_{qa}(n)$, and Laplacian kernel function is K_n. $\sigma_q(n)$ and $\mu_q(n)$ are autocorrelation factor and designed parameter, respectively, which give an additional degree of freedom.

The μ_q and K_n are described as,

$$K_n\left(\mu_q(n), \sigma_q(n)\right) = e^{-\Omega \times \left\| \mu_q(n) - \sigma_q(n) \right\|} \tag{21}$$

$$\mu_q(n+1) = \tau \times \mu_q(n) + \varsigma \times \left(\sigma_q(\mathrm{n}+1)\right)^2 \tag{22}$$

Where, τ and ς are accelerating parameters.

The $\sigma_q(n)$ is defined as,

$$\sigma_q(n+1) = \vartheta \times \sigma_q(n) + (1-\vartheta) \times \phi_{aqe}(n) \times \phi_{aqe}(n-1) \tag{23}$$

i_{ssqa} is calculated as,

$$i_{ssqa} = L_{aq} \times u_{qs} \tag{24}$$

For easy implementation, the block model of GDLSR, for $L_{qa}(n)$ and i_{ssqa} generation is shown in Fig.4.

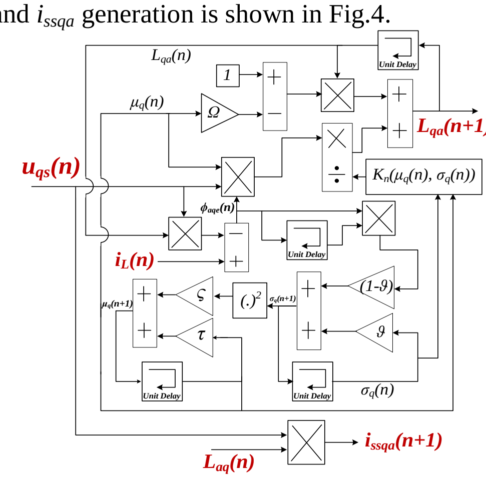

Fig.4 Block model of GDLSR for the reactive weight component.

Fig. 5 presents the block diagram of GDLSR based NN structure for active and reactive filtered conductance weight calculation process. The process of GDLSR based control technique is described through flowchart, which is shown in Fig.6.

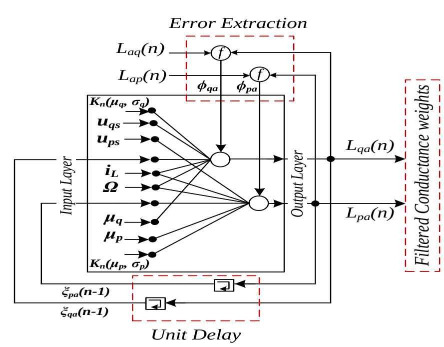

Fig.5 Block diagram of GDLSR-based NN Structure.

This article has been accepted for publication in a future issue of this journal, but has not been fully edited. Content may change prior to final publication. Citation information: DOI 10.1109/TIE.2018.2886765, IEEE Transactions on Industrial Electronics

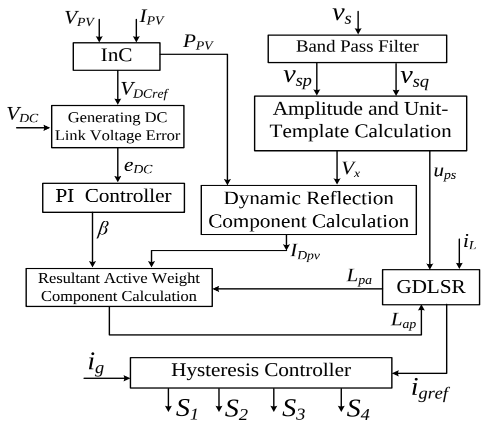

Fig.6 Flowchart of GDLSR-based control technique.

IV. Results and Discussion

A prototype of the system is developed for performance evaluation of GDLSR based control technique, as shown in Fig.7.

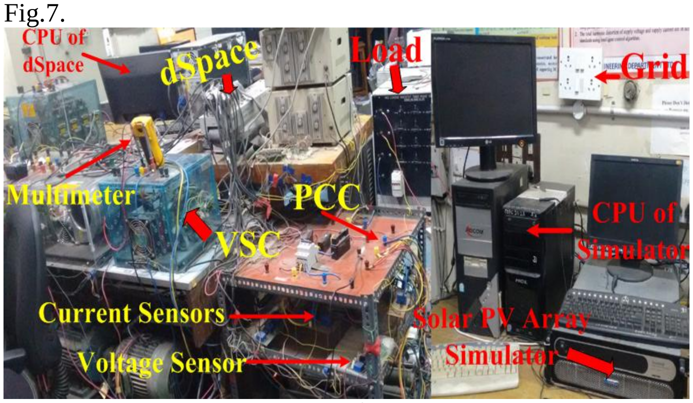

Fig.7 Photograph of the prototype.

To realize the PV characteristic, a solar PV simulator (AMETEK, ETS600x17DPVF) is used, and it is integrated to the main grid. During integration, for PV power conversion into AC form, load feeding, and synchronization, a single-phase VSC is used. The RC filter and interfacing inductor, are used for harmonics and switching ripples mitigation. A DSpace (Digital Signal Processor for Applied and Control Engineering) controller (1202-DSPACE) is used for execution of control techniques. Hall-Effect current (LA-55p) and voltage (LV-25) sensors are used for sensing all signals. For voltage and current measurement, a multimeter (Fluke-115) is used. A power quality analyzer (Fluke-43B) is used for analysis of harmonic spectra of current and voltage. Differential voltage probes (HAMEG-115Hz) and current probes (Tektronix-A622) are used for voltage and current measurement. A digital storage oscilloscope (DSO7014A) is used for recording dynamic performance. In Table I, the system parameters are given.

TABLE I
SYSTEM PARAMETERS

Parameter	Value	Parameter	Value	Parameter	Value	Parameter	Value
I_{sc}	6A	P_{Load}	800W	F	50Hz	v_s	154.4V
V_{oc}	250V	$\Delta\xi$	2V	C_{fl}	10μF	ς	0.00001
V_{mpp}	215.4V	Ω	0.0002	R_{fl}	10Ω	Γ	1
I_{mpp}	5.688A	ϑ	0.2	L_{ln}	5mH	G_P, G_{Pa}	0.1
P_{mpp}	1.224kW	τ	0.001	R_{ln}	0.5Ω	G_I, G_{Ia}	0.001

A. *Operation at Nonlinear Loads*

Here, it is assumed that the produced solar PV power is more than the load demand. Therefore, after meeting the load demand, the rest power is supplied to the grid. During power feeding into the grid, different adverse conditions are considered such as, grid under-voltage, grid overvoltage and distorted v_s condition. However, the main task is to, maintain the power quality and %THD [27][28] of i_g is under the acceptable limit, according to the IEEE-519 standard [29].

1) *Operation under normal grid voltage condition*

The steady-state responses under normal v_s condition, are illustrated in Figs.8-10, where a nonlinear load is connected at PCC.

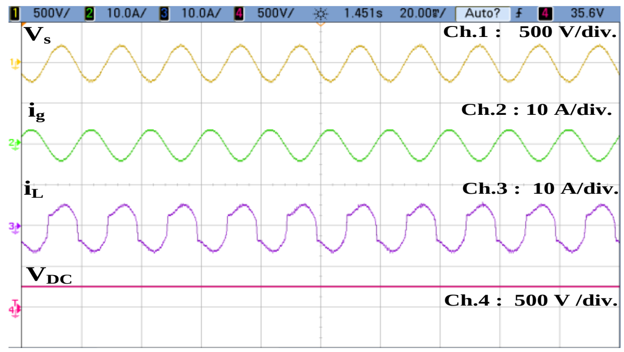

Fig.8 Waveforms under normal condition.

In Fig.8, i_g and v_s are out of phase from each other, which shows that after meeting the load demand, the rest solar power is fed to the grid, and V_{DC} is maintained at the required value. Moreover, the square waveform of i_L depicts that load is highly nonlinear in nature.

Fig.9(b) shows that after meeting the load demand, extra 409W power is fed to the grid. In Figs.9(c)-(d), the harmonic spectra of v_s and i_g show that the THD of the grid voltage and current are 1.2% and 1.4%, which is well within the permissible limit of 5% according to the IEEE-519 standard. Moreover, in Fig.9(a), i_g and v_s are out of phase from each other, as well as in Fig.9(b) negative power, shows that extra P_{PV} is supplied to the grid.

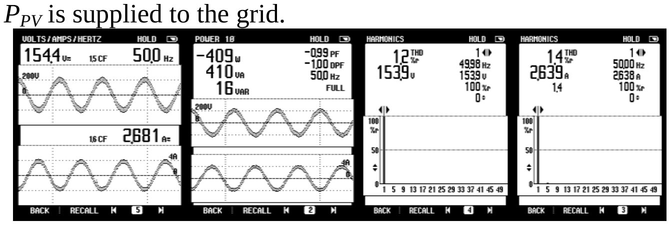

(a) (b) (c) (d)

Fig.9 Waveforms of (a) v_s and i_g, (b) power fed into grid, (c) harmonic spectrum of v_s, and (d) harmonic spectrum of i_g.

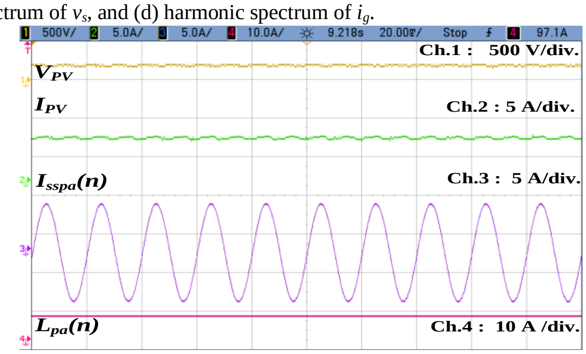

Fig.10 Waveforms of PV and load components.

This article has been accepted for publication in a future issue of this journal, but has not been fully edited. Content may change prior to final publication. Citation information: DOI 10.1109/TIE.2018.2886765, IEEE Transactions on Industrial Electronics

In Fig.10, the waveforms of V_{PV} and I_{PV} at solar insolation 1000W/m^2 are given, which shows a good tracking behaviour behaviour. Moreover, the waveforms of $i_{sspa}(n)$ and $L_{Pa}(n)$, which are extracted from i_L by using GDLSR based control algorithm are given in Fig.10. The sinusoidal waveform of $i_{sspa}(n)$, and constant $L_{Pa}(n)$, show the strong estimation ability of GDLSR algorithm.

2) *Operation at grid over-voltage*

During testing for grid voltages fluctuation, at over voltage condition, the fluctuation in grid voltage of approximately 20% is taken, which test responses are shown in Fig.11.

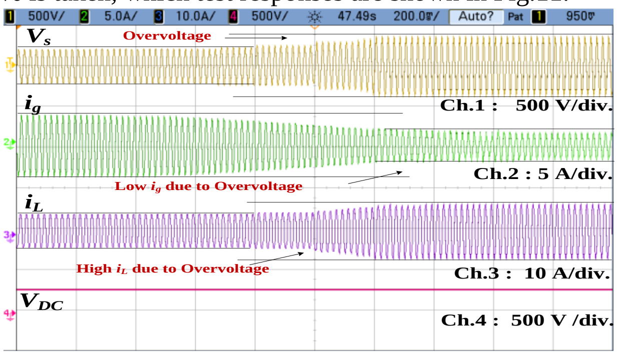

Fig.11 Waveforms during overvoltage condition.

Moreover, harmonics spectra of grid current and grid voltage are shown in Fig.12. The waveforms at over-voltage depict that, the v_s at PCC is increased, so due to constant supply power, the i_g is decreased. Moreover, since P_L (load power) is directly propositional to the square of v_s, so P_L, as well as i_L, is increased. However, due to strong control ability, the V_{DC} is regulated to required value, and a balanced power is fed to the load, which is shown in Fig.11. Moreover, after meeting the load demand, the extra power is supplied to the grid. During this process, the THD of i_g is still low and within the permissible limit of 5% according to the IEEE-519 standard, which is shown in Fig.12. The achieved %THD of i_g and v_s are 2.4% and 2.3%, as well as the value of i_g and v_s are 2.26A and 180V, which are shown in Figs.12(a)-(c).

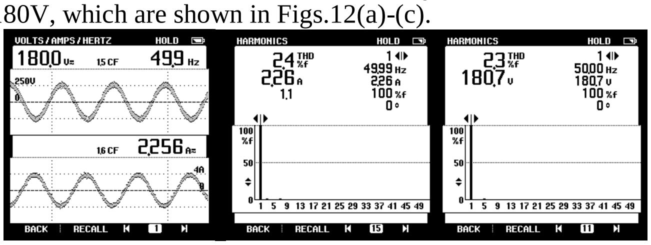

(a) (b) (c)

Fig.12 Waveforms of, (a) v_s and i_g, (b)-(c) harmonic spectrum of i_g and v_s, under the condition of grid overvoltage.

3) *Operation at grid under-voltage*

During testing at grid under-voltage condition, the fluctuation in grid voltage of approximately 15% is taken, which test responses are shown in Fig.13. Moreover, harmonics spectra of grid current and PCC voltage are shown in Fig.14. The waveforms at under-voltage depict that the v_s at PCC is decreased, so due to constant supply power, the i_g is increased. Moreover, since P_L is directly propositional to the square of v_s, so i_L is decreased. However, due to strong control ability, the V_{DC} is maintained to required value, and a balanced power is fed to the load, which is shown in Fig.13. Moreover, after fulfil the load demand, the extra power is supplied to the grid. During this process, the THD of i_g is still low and within the permissible limit of 5% according to the IEEE-519 standard, which is shown in Fig.14. The achieved %THD of i_g and v_s are 2.6% and 2.1%, as well as the value of i_g and v_s are 3.328A and 122.9V, which are shown in Figs.14(a)-(c).

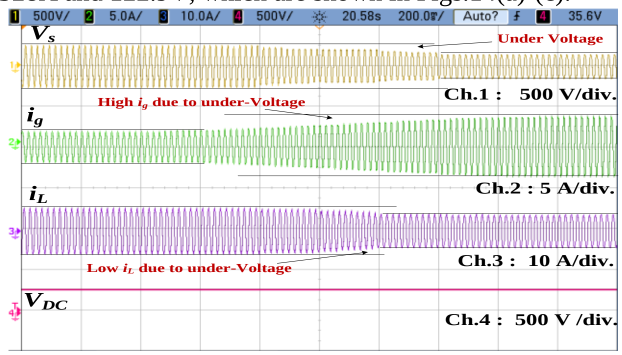

Fig.13 Waveforms under the condition of grid under-voltage.

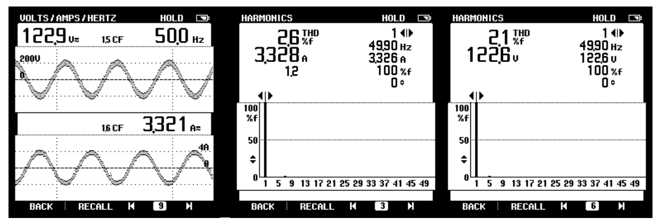

(a) (b) (c)

Fig.14 Waveforms of, (a) v_s and i_g, (b)-(c) harmonic spectrum of i_g and v_s, under grid under-voltage condition.

4) *Operation at distorted grid voltage condition*

Performances under distorted v_s condition are shown in Fig.15, and analyzed by using a power analyzer, which obtained waveforms are shown in Fig.16.

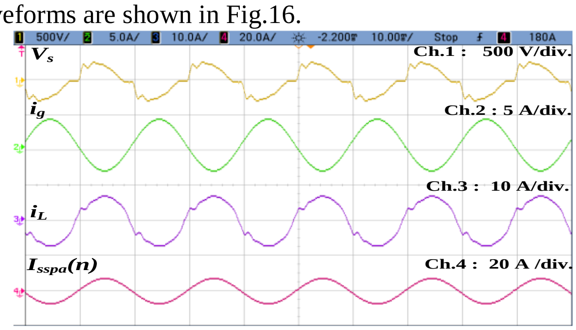

Fig.15 Waveforms under distorted V_s condition.

Here THD of distorted v_{ga} is 7.8%, which is shown in Fig.16(c). Moreover, at PCC, the nonlinear load is attached. In this highly nonlinear situation, the proposed control technique has performed very well and properly fed the load. After fulfil the load demand, the extra power is successfully transferred to the grid, where THD of i_g is only 2.1%, at unity power factor, which is shown in Fig.16(d). The waveforms of v_s, i_g and power, are shown in Figs.16(a)-(b).

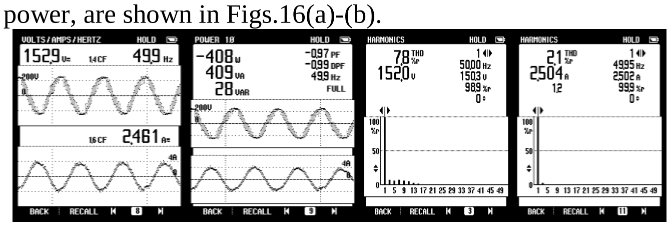

(a) (b) (c) (d)

Fig.16 Waveforms of, (a) v_s and i_g, (b) power supply into the grid, (c) harmonic spectrum of v_s and (c) i_g.

This article has been accepted for publication in a future issue of this journal, but has not been fully edited. Content may change prior to final publication. Citation information: DOI 10.1109/TIE.2018.2886765, IEEE Transactions on Industrial Electronics

5) Comparative Analysis under Distorted Grid Voltage and Nonlinear Load Condition

For comparative analysis, on same circuitry condition, SRFT, LMS and proposed GDLSR techniques are tested. During testing, the nonlinear load is attached, at PCC and distorted grid voltage situation is taken, which harmonic spectra are shown in Fig.17(a) and Fig.17(b). The THD of i_L and v_s are 18.9% and 7.8%, respectively. In this highly nonlinear condition, the objectives of the controllers are, first the load demand is fulfilled, and after that the rest power is fed to the grid at unity power factor. In this situation, the obtained harmonic spectrum of i_g shows that the achieved THD of i_g by using SRFT based control technique is very poor, that is 4.9%, which is shown in Fig.18(a). In the case of LMS based control technique, the THD of i_g is improved, that is 4.4%, which is shown in Fig.18(b). However, Fig.18(c) shows that the obtained THD of i_g by using GDLSR technique is only 2.2%, which depicts a significant difference, in comparison to state of art techniques.

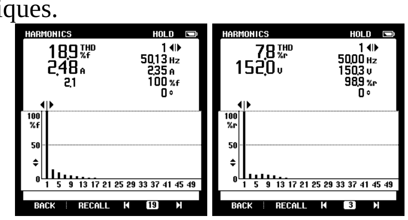

(a) (b)

Fig. 17 Harmonic spectra of, (a) i_L, and (b) v_s.

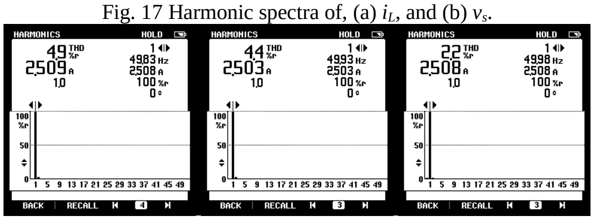

(a) (b) (c)

Fig. 18 Harmonic spectrum of i_g, using (a) SRFT, (b) LMS, and (c) GDLSR.

B. Operation during Solar Insolation Variation Condition

During the insolation variation condition, it is tested for insolation rise, as well as tested for insolation fall. In this condition, insolation jumps from 800W/m^2 to 1000W/m^2, which steady-state performances are shown in Fig.19.

Fig.19 shows that in both conditions, the tracking efficiency is approximately close to 100%.

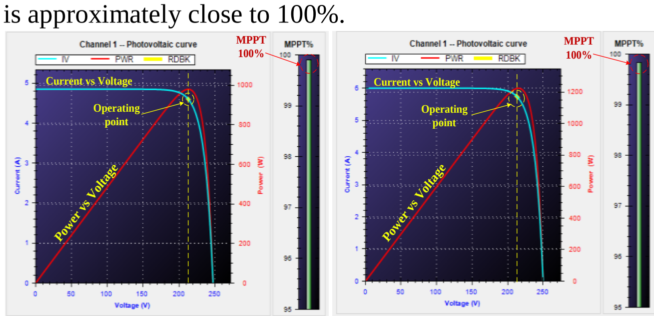

(a) (b)

Fig.19 steady state performance at (a) 800W/m^2 and (b) 1000W/m^2 .

1) Operation during irradiation rise

During irradiation rise condition, an increase in solar insolation from 800W/m^2 to 1000W/m^2 is considered, which output waveforms are shown in Fig.20.

Fig.20 shows that an InC technique has tracked very smoothly the maximum power point, as well as in this operation, the i_L is constant, and V_{DC} is increased. Because, in single stage topology, PV array is directly attached to DC link. Moreover, a dynamic reflection component is used in control, which enhances the performance during dynamic condition.

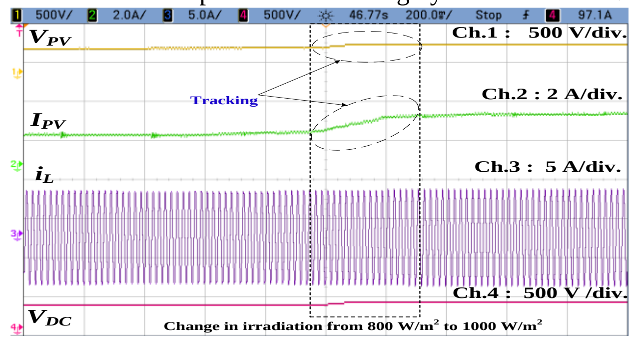

Fig.20 Waveform during insolation rise.

2) Operation during irradiation fall

During irradiation fall condition, a decrease in solar insolation from 1000W/m^2 to 800W/m^2 is considered, which output waveforms are shown in Fig.21.

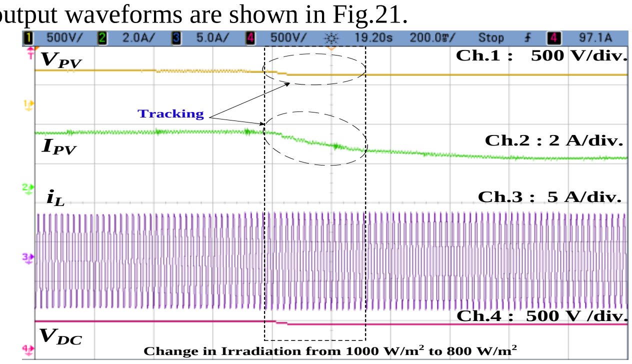

Fig.21 Waveform during insolation fall.

Fig.21 shows that maximum power point is reached using an InC algorithm, as well as in this operation, the i_L is constant, and V_{DC} is decreased. Because, in single stage topology, DC link is directly attached to PV array.

C. Operation during Day-to-Night Condition

In day-to-night condition, during the daytime, solar PV power is used to fulfil the load demand, and if some power is left, then it is fed into the grid. Moreover, during the night time, when the solar power is zero, then the load demand is fulfilled by taking power from the grid, and VSC acts as a DSTATCOM, which provides reactive power support. These performances for day-to-night mode, are shown in Figs.22-24.

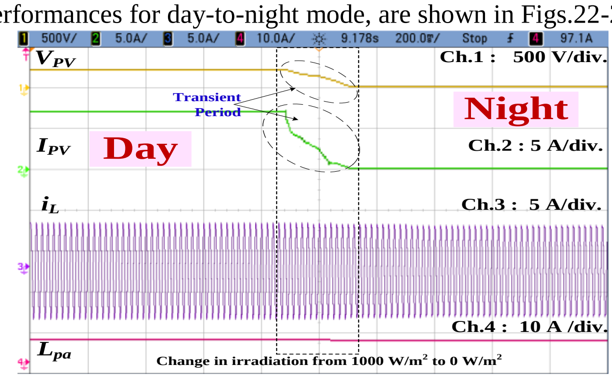

Fig.22 Waveforms of PV during day-to-night condition.

This article has been accepted for publication in a future issue of this journal, but has not been fully edited. Content may change prior to final publication. Citation information: DOI 10.1109/TIE.2018.2886765, IEEE Transactions on Industrial Electronics

In Fig.23, during the daytime, i_g and v_s are out of phase, which shows that the power is fed into the grid. Moreover, in Fig.23 and Fig.24 during night time, i_g and v_s are in the same phase, which shows that power is supplied from the grid. In both conditions, the V_{DC} is maintained to required value, which has only possible due to the strong controlling ability of the GDLSR based VSC control.

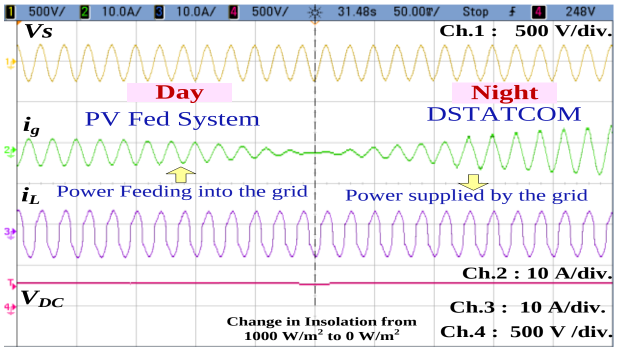

Fig.23 Waveforms of grid and load during day-to-night condition.

The waveforms of I_{PV} and V_{PV} in both situations are shown in Fig.22, which shows that i_L is constant. Because during mode change, P_{PV} decreases continually and when P_{PV} is less than the P_L, then the grid starts supplying power to the load. The waveforms of power quality analysis, during DSTATCOM mode of operation, are shown in Fig.24, which shows that the %THDs of v_s and i_g are 2.1% and 2.2%. A comparative analysis of proposed technique with the popular state of the art technique is given in Table II, which shows that the proposed GDLSR based technique is superior w.r.t. other techniques. However, the algorithm complexity of GDLSR based control technique is high. Therefore, for easy implementation and to reduce the algorithm complexity, the block diagrams of GDLSR for active and reactive component are given in Fig.3 and Fig.4, respectively, as well as flowchart is given in Fig.6. Moreover, in the case of GDLSR technique, the requirement of the cache memory is slightly high w.r.t. SRFT technique, but w.r.t. LMS technique, the requirement of the cache memory is less. Therefore, the proposed GDLSR based control technique, fulfils the motive of the work.

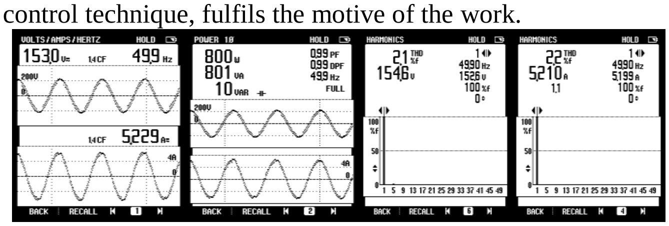

(a) (b) (c) (d)

Fig.24 Waveforms during DSTATCOM operation, (a) v_s and i_g, (b) supply power, (c)-(d) harmonic spectrum of v_s and i_g.

TABLE II: COMPARATIVE ANALYSIS OF PROPOSED NN BASED ALGORITHM WITH CONVENTIONAL ALGORITHM

Parameter	Proposed Algorithm	SRFT [9]	LMS [7]
No. of Computation	Low	High	Low
DC link Voltage Oscillation	Low	High	Medium
Accuracy	High	Medium	Poor
THDs in Grid Current	Low	Medium	Medium
DSP Speed	High	Low	High
Sampling Time	30µs	40µs	30µs
Algorithm Complexity	High	Low	Medium
Requirement of Cache Memory	Medium	Low	High

V. CONCLUSION

A novel control technique namely gradient descent least squares regression (GDLSR) based NN control algorithm for grid-integrated solar PV system has been developed. This single layer GDLSR-based NN structure has a very simple architecture, which reduces the computational burden and algorithm complexity. Therefore, it is easy in implementation. The performance of proposed NN based control technique has been evaluated under abnormal conditions, such as, over-voltage, under-voltage, distortion in the grid voltage, nonlinear loading and solar irradiation variation. Experimental results have shown satisfactory performance of its operation at unity power factor under every types of abnormal conditions. Moreover, the THDs of grid voltage and grid current have been observed within the IEEE-519 standard.

REFERENCES

[1] F. Lamberti, V. Calderaro, V. Galdi, and G. Graditi, “Massive data analysis to assess PV/ESS integration in residential unbalanced LV networks to support voltage profiles,” *Electric Power Systems Research*, vol. 143, pp. 206-214, Feb. 2017.

[2] K. Kiran Prasad, H. Myneni and S. K. Ganjikunta, "Power Quality Improvement and PV Power Injection by DSTATCOM with Variable DC Link Voltage Control from RSC-MLC," *IEEE Trans. Sustainable Energy*, 2018, (Early Access).

[3] F. Lin, K. Lu and B. Yang, "Recurrent Fuzzy Cerebellar Model Articulation Neural Network Based Power Control of a Single-Stage Three-Phase Grid-Connected Photovoltaic System During Grid Faults," *IEEE Trans. Ind. Electronics*, vol. 64, no. 2, pp. 1258-1268, Feb. 2017.

[4] F. J. Lin, K. C. Lu and B. H. Yang, "Recurrent Fuzzy Cerebellar Model Articulation Neural Network Based Power Control of a Single-Stage Three-Phase Grid-Connected Photovoltaic System During Grid Faults," *IEEE Trans. Ind. Electronics*, vol. 64, no. 2, pp. 1258-1268, Feb. 2017.

[5] M. Valtierra-Rodriguez, R. de Jesus Romero-Troncoso, R. A. Osornio-Rios and A. Garcia-Perez, "Detection and Classification of Single and Combined Power Quality Disturbances Using Neural Networks," *IEEE Trans. Industrial Electronics*, vol. 61, no. 5, pp. 2473-2482, May 2014.

[6] S. Haykin, *Neural Networks and Learning Machines*, 3rd ed. Upper Saddle River, NJ, USA: Pearson Education, 2009.

[7] S. Xie, W. Zhong, K. Xie, R. Yu, and Y. Zhang, “Fair energy scheduling for vehicle-to-grid networks using adaptive dynamic programming,” *IEEE Trans. Neural Netw. Learn. Syst*., vol. 27, no. 8, pp. 1697–1707, Aug. 2016.

[8] S. Mishra, “Neural-network-based adaptive UPFC for improving transient stability performance of power system,” *IEEE Trans. Neural Netw.*, vol. 17, no. 2, pp. 461–470, Mar. 2006.

[9] R. K. Agarwal, I. Hussain and B. Singh, "Application of LMS-Based NN Structure for Power Quality Enhancement in a Distribution Network Under Abnormal Conditions," *IEEE Trans. Neural Networks and Learning Systems*, vol. 29, no. 5, pp. 1598-1607, May 2018.

[10] G. K. Venayagamoorthy, R. K. Sharma, P. K. Gautam, and A. Ahmadi, “Dynamic energy management system for a smart microgrid,” *IEEE Trans. Neural Netw. Learn. Syst.*, vol. 27, no. 8, pp. 1643–1656, Aug. 2016.

[11] S. Somkun and V. Chunkag, “Unified Unbalanced Synchronous Reference Frame Current Control for Single-Phase Grid-Connected Voltage-Source Converters,” *IEEE Trans. Industrial Electronics*, vol. 63, no. 9, pp. 5425-5436, Sept. 2016.

[12] B. P. McGrath, D. G. Holmes and J. J. H. Galloway, "Power converter line synchronization using a discrete Fourier transform (DFT) based on a variable sample rate," *IEEE Trans. Power Electronics*, vol. 20, no. 4, pp. 877-884, July 2005.

[13] J. Zygarlicki, M. Zygarlicka, J. Mroczka and K. J. Latawiec, "A Reduced Prony's Method in Power-Quality Analysis—Parameters Selection," *IEEE Trans. Power Delivery*, vol. 25, no. 2, pp. 979-986, April 2010.

[14] S. K. Chaudhary, R. Teodorescu, P. Rodriguez, P. C. Kjaer and A. M. Gole, “Negative Sequence Current Control in Wind Power Plants With VSC-HVDC Connection,” *IEEE Trans. Sus. Energy*, vol. 3, no. 3, pp. 535-544, July 2012.

[15] G. Rigatos, P. Siano, N. Zervos and C. Cecati, "Decentralised control of parallel inverters connected to microgrid using the derivative-free non-linear Kalman filter," *IET Power Elect.*, vol. 8, no. 7, pp. 1164-1180, July 2015.

[16] A. Vidal, F. D. Freijedo, A. G. Yepes, J. Malvar, Ó. López and J. Doval-Gandoy, "Transient response evaluation of stationary-frame resonant current controllers for grid-connected applications," *IET Power Electronics*, vol. 7, no. 7, pp. 1714-1724, July 2014.

[17] Y. Tang, H. He, Z. Ni, J. Wen and T. Huang, "Adaptive Modulation for DFIG and STATCOM With High-Voltage Direct Current Transmission," *IEEE Trans. Neural Networks and Learning Systems*, vol. 27, no. 8, pp. 1762-1772, Aug. 2016.

[18] B. Widrow, J. M. McCool, M. G. Larimore and C. R. Johnson, "Stationary and nonstationary learning characteristics of the LMS adaptive filter," *Proc. of IEEE*, vol. 64, no. 8, pp. 1151-1162, Aug. 1976.

[19] R. K. Agarwal, I. Hussain and B. Singh, "LMF-Based Control Algorithm for Single Stage Three-Phase Grid Integrated Solar PV System," *IEEE Trans. Sustainable Energy*, vol. 7, no. 4, pp. 1379-1387, Oct. 2016.

[20] R. K. Agarwal, I. Hussain and B. Singh, "Implementation of LLMF Control Algorithm for Three-Phase Grid-Tied SPV-DSTATCOM System," *IEEE Trans. Industrial Electronics*, vol. 64, no. 9, pp. 7414-7424, Sept. 2017.

[21] M. R. Hajiaboli, M. O. Ahmad and C. Wang, "An Edge-Adapting Laplacian Kernel For Nonlinear Diffusion Filters," *IEEE Trans. Image Processing*, vol. 21, no. 4, pp. 1561-1572, April 2012.

[22] M. Jafari, S. B. Naderi, M. T. Hagh, M. Abapour and S. H. Hosseini, "Voltage Sag Compensation of Point of Common Coupling (PCC) Using Fault Current Limiter," *IEEE Trans. Power Delivery*, vol. 26, no. 4, pp. 2638-2646, Oct. 2011.

[23] C. Kumar, M. K. Mishra and M. Liserre, "Design of External Inductor for Improving Performance of Voltage-Controlled DSTATCOM," *IEEE Trans. Industrial Electronics*, vol. 63, no. 8, pp. 4674-4682, Aug. 2016.

[24] A. Safari and S. Mekhilef, "Simulation and Hardware Implementation of Incremental Conductance MPPT With Direct Control Method Using Cuk Converter," *IEEE Trans. Industrial Electronics*, vol. 58, no. 4, pp. 1154-1161, April 2011.

[25] K. H. Leung, K. H. Loo and Y. M. Lai, "Unity-Power-Factor Control Based on Precise Ripple Cancellation for Fast-Response PFC Preregulator," *IEEE Trans. Power Electronics*, vol. 31, no. 4, pp. 3324-3337, April 2016.

[26] N. Kumar, I. Hussain, B. Singh and B. K. Panigrahi, "Implementation of Multilayer Fifth-Order Generalized Integrator-Based Adaptive Control for Grid-Tied Solar PV Energy Conversion System," *IEEE Trans. Industrial Informatics*, vol. 14, no. 7, pp. 2857-2868, July 2018.

[27] N. Yousefpoor, S. H. Fathi, N. Farokhnia and H. A. Abyaneh, "THD Minimization Applied Directly on the Line-to-Line Voltage of Multilevel Inverters," *IEEE Trans. Industrial Electronics*, vol. 59, no. 1, pp. 373-380, Jan. 2012.

[28] N. Kumar, I. Hussain, B. Singh and B. K. Panigrahi, "Normal Harmonic Search Algorithm Based MPPT for Solar PV System and Integrated with Grid using Reduced Sensor Approach and PNKLMS Algorithm," *IEEE Trans. Industry Applications,* 2018. (Early Access).

[29] C. K. Duffey and R. P. Stratford, "Update of harmonic standard IEEE-519: IEEE Recommended Practices and Requirements for Harmonic Control in Electric Power Systems," *Record of Conference Papers., Industrial Applications Society 35th Annual Petroleum and Chemical Industry Conference,*, Dallas, TX, 1988, pp. 249-255.

Nishant Kumar (M'15), received the M.Tech. (Gold Medalist) degree in electrical power system from the National Institute of Technology Durgapur, Durgapur, WB, India, in 2013. He is currently working toward the Ph.D. degree in power system in the Department of Electrical Engineering, Indian Institute of Technology (IIT) Delhi, New Delhi, India.

From 2013 to 2014, he was the Project Engineer/Research Associate with IIT Bombay and IIT Delhi. His areas of research interests include soft computing based generation control, optimization algorithm development, and application of soft computing techniques in power system planning, operation and control.

He has received Gold Medal in M.Tech degree from National Institute of Technology Durgapur, India in the year 2013, and POSOCO Power System National Award (PPSA-2018) in Doctoral Category, from Power Grid Corporation of India Limited, in the year 2018.

Bhim Singh (SM'99, F'10) was born in Rahamapur, Bijnor, UP, India, in 1956. He received the B.E. degree in electrical from the University of Roorkee, Roorkee, India, in 1977, and the M.Tech. degree in power apparatus and systems and the Ph.D. degree in electrical machine from Indian Institute of Technology (IIT) Delhi, New Delhi, India, in 1979 and 1983, respectively.

In 1983, he joined the Department of Electrical Engineering, University of Roorkee (now IIT Roorkee), as a Lecturer. He became a Reader there in 1988. In December 1990, he joined the Department of Electrical Engineering, IIT Delhi, as an Assistant Professor, where he has become an Associate Professor in 1994 and a Professor in 1997. He has been the Head in the Department of Electrical Engineering, IIT Delhi, from July 2014 to August 2016. He is currently the Dean, Academics with IIT Delhi. He has guided 70 Ph.D. dissertations, 161 M.E./M.Tech./M.S.(R) thesis. He has executed more than 75 sponsored and consultancy projects.

His areas of research interests include PV grid interface systems, microgrid, power quality, PV water pumping systems, power electronics, electrical machines, drives, FACTS, and HVdc systems.

Bijaya Ketan Panigrahi (SM'06) received the Ph.D. degree in power system from Sambalpur University, Sambalpur, India, in 2004.

He was a Lecturer with the University College of Engineering, Sambalpur, for 13 years. Since 2005, he has been an Associate Professor in the Department of Electrical Engineering, Indian Institute of Technology (IIT) Delhi, New Delhi, India, where he has become a Professor in 2017.

His research interests include intelligent control of flexible ac transmission system devices, digital signal processing, power quality assessment, and application of soft computing techniques to power system planning, operation and control.